

**Anomalous pairing vibration in neutron-rich Sn isotopes beyond the  $N = 82$  magic number**

Hirotaka Shimoyama and Masayuki Matsuo

*Department of Physics, Faculty of Science and Graduate School of Science and Technology, Niigata University, Niigata 950-2181, Japan*

(Received 3 June 2011; published 19 October 2011)

Two-neutron transfer associated with the pair correlation in superfluid neutron-rich nuclei is studied with focus on low-lying  $0^+$  states in Sn isotopes beyond the  $N = 82$  magic number. We describe microscopically the two-neutron addition and removal transitions by means of the Skyrme-Hartree-Fock-Bogoliubov mean-field model and the continuum quasiparticle random phase approximation formulated in the coordinate space representation. It is found that the pair transfer strength for the transitions between the ground states becomes significantly large for the isotopes with  $A \geq 140$ , reflecting very small neutron separation energy and long tails of the weakly bound  $3p$  orbits. In  $^{132-140}\text{Sn}$ , a peculiar feature of the pair transfer is seen in transitions to low-lying excited  $0^+$  states. They can be regarded as a kind of pair vibrational mode which is characterized by an anomalously long tail of the transition density extending to far outside of the nuclear surface, and a large strength comparable to that of the ground-state transitions. The presence of the weakly bound neutron orbits plays a central role for these anomalous behaviors.

DOI: [10.1103/PhysRevC.84.044317](https://doi.org/10.1103/PhysRevC.84.044317)

PACS number(s): 21.10.Pc, 21.10.Re, 21.60.Jz, 25.40.Hs

**I. INTRODUCTION**

Recently two-neutron transfer processes have attracted renewed interests thanks to the opportunities of two-neutron transfer reaction experiments using the beams of radioactive neutron-rich isotopes [1–5]. In the past a considerable number of experimental and theoretical studies of two-neutron transfer have been accumulated for stable nuclei [6–12]. One of the central concepts established there is that the two-neutron transfer amplitude is influenced by collective excitation modes caused by the superfluidity or the pair correlation [7–9,12]. In the case of open-shell nuclei, the strong two-neutron transfer transitions connecting the ground states emerge; it is a Nambu-Goldstone mode related to the rotational symmetry with respect to the phase of the pair condensate, called the pairing rotation. The pairing vibration, which corresponds to a vibration of the pairing gap, is another collective mode producing a low-lying excited  $0^+$  state, but the intensity of the associated pair transfer is significantly smaller than the pairing rotation [8,12].

When neutron-rich nuclei are concerned, the above conventional picture of the pairing collectivity may be modified. We can expect this because neutron-rich nuclei often accompany skin or halo, that is, low density distributions of weakly bound neutrons surrounding the nucleus, and also because the neutron pairing in neutron matter is predicted to be strong or close to the strong-coupling regime at low densities [13–19]. The expected enhancement of the pair correlation may result in unusual properties in two-neutron transfers. Dobaczewski *et al.* [20] has pointed out the possibility that the two-neutron transfer associated with the pairing rotation may be enhanced in neutron-rich nuclei because of the surface enhanced pairing. Influences of the surface enhancement on the pair vibrational two-neutron transfer populating excited  $0^+$  states and the first  $2^+$  states in neutron-rich Sn isotopes are discussed in Refs. [21,22] and in Ref. [23], respectively. Recent experiments of  $(p, t)$  reaction on light-mass neutron-rich nuclei such as  $^7\text{Li}$  [2,24,25] and  $^6,8\text{He}$  [1,3–5] point to the

importance of the pair correlation in these typical halo or skin nuclei. The giant pairing vibration in neutron-rich nuclei has also been discussed [26,27].

In the present paper we study the pairing collective modes in heavy-mass neutron-rich nuclei in order to explore new features in the pairing rotation, the pairing vibration, and the associated two-neutron transfer amplitudes. We focus on excitation modes with monopole multipolarity ( $L = 0$ ), for which the strong pairing collectivity is expected. We analyze the Sn isotopic chain ranging from the proton-rich side  $^{100}\text{Sn}$  ( $N = 50$ ) to very neutron-rich isotopes with  $A \sim 150$  beyond the  $N = 82$  magic number ( $^{132}\text{Sn}$ ). Our theoretical tool is the Hartree-Fock-Bogoliubov mean-field model using the Skyrme energy density functional and the continuum quasiparticle random phase approximation, and it is the same as adopted in Ref. [23]. A similar approach is taken by Khan *et al.* [21,26], where the  $L = 0$  pairing vibration in neutron-rich Sn isotopes is also studied. Compared with Ref. [21], we perform more systematic and detailed analyses, which eventually bring us a new finding and some differences. Among all, the present analysis predicts an anomalous pairing vibration in  $^{134-140}\text{Sn}$ , which we will explain below.

**II. SKYRME-HARTREE-FOCK-BOGOLIUBOV MEAN-FIELD PLUS QRPA APPROACH****A. The model**

We describe the neutron pair correlation by means of the Hartree-Fock-Bogoliubov (HFB) mean-field theory [28] and the continuum quasiparticle random phase approximation (QRPA) [29,30]. We assume the spherical symmetry of the mean fields and densities associated with the ground states of the subshell-closed Sn isotopes. The model adopted in the present study is the same as that in Ref. [23].

The starting point of the model is the energy density functional, which we construct from the Skyrme interaction with the parameter set SLy4 [31], and the density-dependent

$\delta$  interaction (DDDI) adopted as an effective pairing force [13,16,20,32–41]. The DDDI is given by

$$v_q^{\text{pair}}(\mathbf{r}, \mathbf{r}') = \frac{1}{2}(1 - P_\sigma)V_q(\mathbf{r})\delta(\mathbf{r} - \mathbf{r}') \quad (q = n, p), \quad (1)$$

where  $V_q(\mathbf{r})$  is the pairing interaction strength and is a function of the neutron and proton densities. We adopt the following form:

$$V_n(\mathbf{r}) = v_0 \left\{ 1 - \eta \left[ \frac{\rho_n(\mathbf{r})}{\rho_c} \right]^\alpha \right\} \quad (2)$$

with the parameters  $v_0 = -458.4 \text{ MeV fm}^3$ ,  $\rho_c = 0.08 \text{ fm}^{-3}$ ,  $\alpha = 0.59$ , and  $\eta = 0.71$  [16,23,39]. Here the parameter  $v_0$  representing the strength in the free space is chosen to reproduce the scattering length  $a = -18.5 \text{ fm}$  of the bare  $nn$  interaction in the  $^1S$  channel, and  $\alpha$  is to fit the density-dependent BCS pairing gap of neutron matter. The parameter  $\eta$  is adjusted so that the calculated average pairing gap  $\Delta_{uv}$  [Eq. (16)] reproduces the experimental pair gap in  $^{120}\text{Sn}$ , which is obtained from the odd-even mass difference using the three-point formula [42]. We call this parameter set DDDI-bare' as it is motivated by the bare nuclear force. This interaction has a strong density dependence. For comparison, we also use the volume pairing interaction ( $v_0 = -195 \text{ MeV fm}^3$  and  $\eta = 0$ ) with no density dependence, and also the mix pairing interaction [36,37] ( $v_0 = -292 \text{ MeV fm}^3$ ) with intermediate density dependence. See Ref. [23] for details. The parameter  $v_0$  of the volume and the mix pairing interactions is determined to reproduce the pair gap in  $^{120}\text{Sn}$ .

The HFB equation is solved in the coordinate space representation using the polar coordinate system. The radial coordinate space is truncated at  $r_{\text{max}} = 20 \text{ fm}$ . The density and the pair density of neutrons or protons are given as sums of the contributions from the quasiparticle states, which we truncate with respect to the angular momentum quantum numbers and the quasiparticle energy. We actually set the maximum orbital angular quantum number  $l_{\text{max}} = 12$  and the maximum quasiparticle energy  $E_{\text{max}} = 60 \text{ MeV}$ .

The excited states are described by means of the QRPA formulated in the coordinate space representation and on the basis of the self-consistent HFB solution. The residual interactions to be used in the QRPA are derived from the Skyrme energy density functional and the DDDI, but the Landau-Migdal approximation is employed for the residual interaction in the particle-hole channel. The Landau-Migdal approximation is good enough in the present analysis since the pair vibration is the collective mode caused mainly by the residual pairing interaction. We have checked numerically that the residual particle-hole interaction gives little influence on the main results.

We impose the outgoing-wave boundary condition on the continuum quasiparticle states in QRPA as described in Refs. [29,30] for the isotopes with  $A \geq 132$ . The box boundary condition is adopted [23] for  $A < 132$ , where the neutron Fermi energy is deeper than  $-6.8 \text{ MeV}$  and the separation energy becomes higher than  $\sim 8 \text{ MeV}$ , in order to save the computational cost for systematic studies. We have checked in a few isotopes with  $A < 132$  that the box boundary condition gives very similar results to those with the outgoing condition. In the QRPA response functions, the

smearing parameter  $\epsilon = 50 \text{ keV}$  is introduced so that the obtained strength function is convoluted with the Lorentzian with the FWHM  $= 2\epsilon = 100 \text{ keV}$ .

## B. Strength function and transition density for pair transfer modes

In the present work we define the strength of the two-neutron transfer using matrix elements of the creation and annihilation operators of a  $S = 0$  pair of neutrons with the angular momentum  $L$ :

$$P_{LM}^\dagger = \int d\mathbf{r} Y_{LM}(\hat{\mathbf{r}}) f(r) \psi_q^\dagger(\mathbf{r} \downarrow) \psi_q^\dagger(\mathbf{r} \uparrow), \quad (3)$$

$$P_{LM} = \int d\mathbf{r} Y_{LM}^*(\hat{\mathbf{r}}) f(r) \psi_q(\mathbf{r} \uparrow) \psi_q(\mathbf{r} \downarrow), \quad (4)$$

where  $f(r)$  is a form factor of the pair-addition and pair-removal operators, and we choose  $f(r) = 1$  in the present analysis for simplicity.

When we consider transitions from the ground state of a nucleus with even  $N$  to states in the neighboring nucleus with  $N + 2$  through the addition of a neutron pair, we evaluate the strength function  $P_{LM}^\dagger$

$$S_{\text{Pad}L}(E) \equiv \sum_{iM} \delta(E - E_{iL}) |\langle \Psi_{iLM} | P_{LM}^\dagger | \Psi_0 \rangle|^2, \quad (5)$$

and for transitions via the removal of a neutron pair we calculate the strength function

$$S_{\text{Prm}L}(E) \equiv \sum_{iM} \delta(E - E_{iL}) |\langle \Psi_{iL-M} | P_{LM} | \Psi_0 \rangle|^2. \quad (6)$$

Here  $\Psi_0$  is the ground state with  $N$  while  $\Psi_{iLM}$  is a state with the angular quantum numbers  $LM$  and the neutron number  $N \pm 2$ , and  $E_{iL}$  is the transition energy measured from the ground state of the residue nucleus with  $N \pm 2$ .

For a specific transition to a given final state populated via the pair-addition and pair-removal operators, the transition densities

$$\begin{aligned} P_i^{(\text{ad})}(\mathbf{r}) &\equiv \langle \Psi_{iLM} | \psi_q^\dagger(\mathbf{r} \downarrow) \psi_q^\dagger(\mathbf{r} \uparrow) | \Psi_0 \rangle \\ &= Y_{LM}^*(\hat{\mathbf{r}}) P_{iL}^{(\text{ad})}(r), \end{aligned} \quad (7)$$

$$\begin{aligned} P_i^{(\text{rm})}(\mathbf{r}) &\equiv \langle \Psi_{iLM} | \psi_q(\mathbf{r} \uparrow) \psi_q(\mathbf{r} \downarrow) | \Psi_0 \rangle \\ &= Y_{LM}(\hat{\mathbf{r}}) P_{iL}^{(\text{rm})}(r), \end{aligned} \quad (8)$$

may be defined. We also evaluate the reduced transition probabilities defined by

$$\begin{aligned} B(\text{Pad}L; \text{gs} \rightarrow i) &\equiv \sum_M |\langle \Psi_{iLM} | P_{LM}^\dagger | \Psi_0 \rangle|^2 \\ &= (2L + 1) \left| \int r^2 P_{iL}^{(\text{ad})}(r) dr \right|^2, \end{aligned} \quad (9)$$

$$\begin{aligned} B(\text{Prm}L; \text{gs} \rightarrow i) &\equiv \sum_M |\langle \Psi_{iL-M} | P_{LM} | \Psi_0 \rangle|^2 \\ &= (2L + 1) \left| \int r^2 P_{iL}^{(\text{rm})}(r) dr \right|^2. \end{aligned} \quad (10)$$

For the procedure to evaluate the strength functions, the transition densities and the transition strengths in the QRPA scheme, we refer the readers to Refs. [23,29,30], in particular, Eqs. (12) and (18) of Ref. [23] for the strength function, and Eqs. (22)–(24) of the same reference for the transition densities.

### III. GROUND-STATE PROPERTIES AND GROUND-STATE TRANSFER

Let us first discuss the monopole transition with  $L = 0$  from the ground state of an even- $N$  isotopes to the ground state of neighboring  $N \pm 2$  isotopes. In the case of superfluid open-shell isotopes the ground-state transfer corresponds to the pairing rotation. With the finite pair gap in the HFB ground state, we can calculate approximately the transition density and the transition matrix element for this transition by neglecting the difference in the configuration in the HFB ground-state wave function [8,12], that is,

$$\begin{aligned} P_{\text{gs}}^{(\text{ad})}(\mathbf{r}) &\equiv \langle \Psi_{0,N+2} | \psi_q^\dagger(\mathbf{r} \downarrow) \psi_q^\dagger(\mathbf{r} \uparrow) | \Psi_0 \rangle \\ &\approx \langle \Psi_0 | \psi_q^\dagger(\mathbf{r} \downarrow) \psi_q^\dagger(\mathbf{r} \uparrow) | \Psi_0 \rangle = \frac{1}{2} \tilde{\rho}(\mathbf{r}), \end{aligned} \quad (11)$$

$$\begin{aligned} P_{\text{gs}}^{(\text{rm})}(\mathbf{r}) &\equiv \langle \Psi_{0,N-2} | \psi_q(\mathbf{r} \uparrow) \psi_q(\mathbf{r} \downarrow) | \Psi_0 \rangle \\ &\approx \langle \Psi_0 | \psi_q(\mathbf{r} \uparrow) \psi_q(\mathbf{r} \downarrow) | \Psi_0 \rangle = \frac{1}{2} \tilde{\rho}(\mathbf{r}), \end{aligned} \quad (12)$$

utilizing the fact that the HFB ground-state  $\Psi_0$  is a mixture of different particles numbers  $N$ ,  $N \pm 2$ , . . . Here  $\tilde{\rho}(\mathbf{r})$  is the pair density defined by

$$\tilde{\rho}(\mathbf{r}) \equiv \langle \Psi_0 | \sum_{\sigma} \psi_q^\dagger(\mathbf{r}\sigma) \psi_q^\dagger(\mathbf{r}\bar{\sigma}) | \Psi_0 \rangle \quad (13)$$

obtained in the HFB calculation. The radial transition density is given as

$$P_{\text{gs}0}^{(\text{ad/rm})}(r) = \sqrt{\pi} \tilde{\rho}(r). \quad (14)$$

In this approximation, there is no distinction between the addition and removal modes. The strength of the ground-state transfer is calculated as

$$B(\text{Pad/rm}0; \text{gs} \rightarrow \text{gs}) = \left| \sqrt{\pi} \int r^2 \tilde{\rho}(r) dr \right|^2. \quad (15)$$

Note that in the closed-shell isotopes  $^{100}\text{Sn}$  and  $^{132}\text{Sn}$  we calculate the strength and the transition density in the QRPA instead of Eqs. (14) and (15) which are not appropriate to nuclei with vanishing pairing gap. In this case, the QRPA reduces to the particle-particle RPA. The ground-state transfer corresponds to the lowest mode of the RPA response.

Figure 1(a) is the plot of the calculated strength  $B(\text{Pad/rm}0)$  of the ground-state two-neutron transfer. The strength is enhanced significantly as the mass number (the neutron number) exceeds  $A = 140$  ( $N = 90$ ). For the isotopes with  $A > 140$ , the absolute magnitude of the pair transfer strength reaches more than twice the maximum strength in the region  $100 < A < 132$ . In the conventional BCS approximation, the

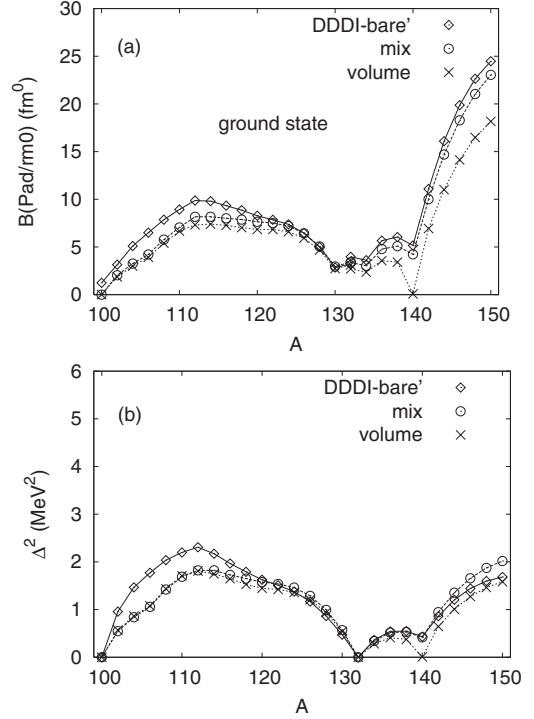


FIG. 1. (a) The neutron pair transfer strength  $B(\text{Pad/rm}0; \text{gs} \rightarrow \text{gs})$  of the ground-state transitions calculated for the even-even Sn isotopes. The diamonds connected with the solid line are the results obtained with the pairing interaction DDDI-bare' while the circles and the crosses are those with the mix and the volume pairing interactions, respectively. (b) The squared average pairing gap  $\Delta_{uv}^2$  of neutrons.

pair transfer strength is proportional to  $(\Delta/G)^2 \propto \Delta^2$  where  $\Delta$  is the pairing gap and  $G$  is the force strength of the seniority pairing force [6,8,12]. In Fig. 1(b) we plot the square  $\Delta_{uv}^2$  of the average pairing gap

$$\Delta_{uv} = \frac{\int \tilde{\rho}(\mathbf{r}) \Delta(\mathbf{r}) d\mathbf{r}}{\int \tilde{\rho}(\mathbf{r}) d\mathbf{r}} \quad (16)$$

of neutrons. Comparing the isotopic trends of the two quantities, we see relative enhancement of the two-neutron transfer strength by a factor of 2 in  $A > 140$ , and also in  $132 < A < 140$ . For the latter isotopes, the absolute magnitude of the average pairing gap is small, but the two-neutron transfer strength is comparable to that of more stable isotopes in the region  $100 < A < 132$ .

The origin of the enhancement is clarified by looking at the pair transition density, which is shown in Figs. 2(a) and 2(b) for  $120 \leq A \leq 132$  and  $132 < A \leq 150$ , respectively. It is seen that the profile of the transition density suddenly changes as the neutron number exceeds the  $N = 82$  magic number and  $N = 90$ . The transition density for  $132 < A \leq 150$  extends outside the surface, reaching  $r \sim 11$  fm for  $132 < A < 140$ , and  $r \sim 14$  fm for  $140 < A < 150$ . The amplitude in the exterior region  $r \gtrsim 7$  fm for  $A \geq 132$  is evidently larger than those for  $A < 132$ , where the amplitudes extend only up to  $r \sim 9$  fm. Comparing the results for  $A = 120$  and for  $A = 144$ , for instance, the maximum values of the amplitude

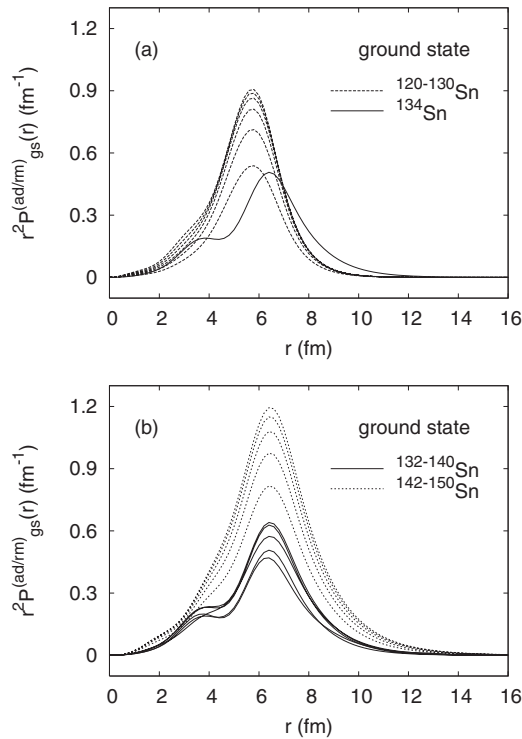


FIG. 2. (a) The neutron pair transition density  $r^2 P_{\text{gs}}^{(\text{ad/rm})}(r)$  for the ground-state transitions in the isotopes  $^{120-130}\text{Sn}$  and  $^{134}\text{Sn}$ . (b) The same as (a), but in  $^{132-140}\text{Sn}$  and  $^{142-150}\text{Sn}$ . The transition density for  $^{132}\text{Sn}$  is the pair-addition transition density  $r^2 P_{\text{gs}}^{(\text{ad})}(r)$  calculated in the QRPA.

around the nuclear surface  $r \sim 6$  fm are approximately the same, but because of the large spatial extension of the transition density, the pair transfer strength in  $^{144}\text{Sn}$  is larger by a factor of  $\sim 2$  (cf. Fig. 1).

The reason for the spatial extension of the pair transition density to develop suddenly beyond  $N = 82$  and  $N = 90$  can be ascribed to the shell gap at  $N = 82$  and properties of the neutron single-particle states. We note here that the transition density of the pair rotational mode, that is, the pair density  $\tilde{\rho}(r)$  is written as a coherent sum of contributions of quasiparticle states, and the quasiparticle states with lower excitation energy (i.e., those originating from orbits close to the Fermi energy) have larger contributions. The calculated Hartree-Fock single-particle energies for neutrons in  $^{132}\text{Sn}$  are  $e_{\text{HF}} = -1.99, -0.25, 0.26$  MeV for the  $2f_{7/2}, 3p_{3/2},$  and  $3p_{1/2}$  orbits located above the  $N = 82$  gap, respectively ( $3p_{1/2}$  is an unbound resonance), and the  $h_{11/2}$  orbit with  $e_{\text{HF}} = -7.68$  MeV is located below the shell gap. For the  $132 < A < 140$  isotopes (where the neutron Fermi energy is located near the position of  $2f_{7/2}$ ), the main component of the transition density originates from this orbit. Since the binding energy of  $2f_{7/2}$  is rather small, the tail of its wave function extends to outside, leading to the long tail in the pair transition density. When the neutron number exceeds  $N = 90$  ( $A = 140$ ), the next single particle orbits  $3p_{3/2}$  and  $3p_{1/2}$  give large contribution to the pair density. Since these  $p$  orbits have very small binding or are unbound, the spatial extension further develops in isotopes with  $N \geq 90$  ( $A \geq 140$ ).

## IV. PAIRING VIBRATION: TRANSFER TO EXCITED STATE

### A. Strength function

We now discuss the two-neutron transfer modes populating excited  $0^+$  states. Figures 3(a)–3(d) show the strength functions  $S_{\text{Pad}0}(E)$  and  $S_{\text{Prm}0}(E)$  for the monopole pair-addition and pair-removal modes in four representative isotopes  $^{102}\text{Sn}$ ,  $^{120}\text{Sn}$ ,  $^{134}\text{Sn}$ , and  $^{142}\text{Sn}$ . Here,  $^{120}\text{Sn}$  is a midshell isotope near the stability line.  $^{134}\text{Sn}$  is a representative of neutron-rich unstable isotope which is located just beyond the neutron magic number  $N = 82$  while  $^{102}\text{Sn}$  has the same closed-shell plus two-particle configuration, but at the neutron-deficient side. In the most neutron-rich isotope  $^{142}\text{Sn}$ , the neutron Fermi energy is located around the weakly bound  $3p_{3/2}$  orbit.

All four isotopes exhibit low-lying peaks in the excitation energy range of  $2 \lesssim E \lesssim 4$  MeV, approximately corresponding to the typical excitation energy  $E \approx 2\Delta$  ( $\sim 2$  MeV) expected to the standard pair vibration model [7,8,12], and they may be regarded as the pair vibration modes. Selecting the peaks with the largest pair-addition strength, the lowest QRPA solution can be identified as the pair-addition vibration in all four cases. Looking at the pair-removal strength, however, the second lowest solution in  $^{120}\text{Sn}$  and  $^{142}\text{Sn}$  can also be identified as the pair vibration, but with the removal character. As typical examples of the pair-addition vibrational modes, we pick up the lowest QRPA solutions in  $^{102}\text{Sn}$ ,  $^{120}\text{Sn}$ , and  $^{134}\text{Sn}$ , and the second lowest solution in  $^{142}\text{Sn}$  as the pair-removal vibration mode.

The most prominent feature seen in Fig. 3 is that the pair-addition strength associated with the low-lying pair vibrational mode in  $^{134}\text{Sn}$  is several times larger than those in the other cases. The pair-addition strength of the pairing vibration is  $B(\text{Pad}0) = 3.16$  in  $^{134}\text{Sn}$  while it is 1.18 and 0.40 in  $^{102}\text{Sn}$  and  $^{120}\text{Sn}$ . The magnitude of the pair addition strength in  $^{134}\text{Sn}$  is so large that it is comparable with the strength  $B(\text{Pad}/\text{rm}0) = 3.61$  associated with the ground-state transition (the pairing rotation). The pair-removal strength is negligibly small, hence it is essentially a pure pair-addition mode. We also notice that the pair vibrational mode in  $^{134}\text{Sn}$  (at  $E = 3.73$  MeV) is located above the one-neutron separation energy  $S_{1n} = 3.31$  MeV (indicated with an arrow in the figure). We estimate the resonance width being less than 1 keV by evaluating the FWHM of the peak minus the smoothing width  $2\epsilon = 100$  keV. The very small width indicates that the pair vibrational state is a *narrow resonance* even though it is embedded in the continuum. The above characteristics indicate clearly that the pair vibrational mode in  $^{134}\text{Sn}$  deviates from the conventional picture of the pairing vibration.

The pair vibrational mode in  $^{142}\text{Sn}$  has a character different from that in  $^{134}\text{Sn}$  as it has the large pair-removal strength instead of the pair-addition strength.

Looking at the strength in  $^{134}\text{Sn}$  and  $^{142}\text{Sn}$  at higher excitation energies, it is seen that there exists a smooth distribution of the pair-addition strength above the two-neutron separation energy  $S_{2n}$ . At any excitation energy above  $S_{2n}$ , it is always possible to put two neutrons outside the nucleus although these two neutrons immediately escape out of the initial position. The smooth distribution can be ascribed to this

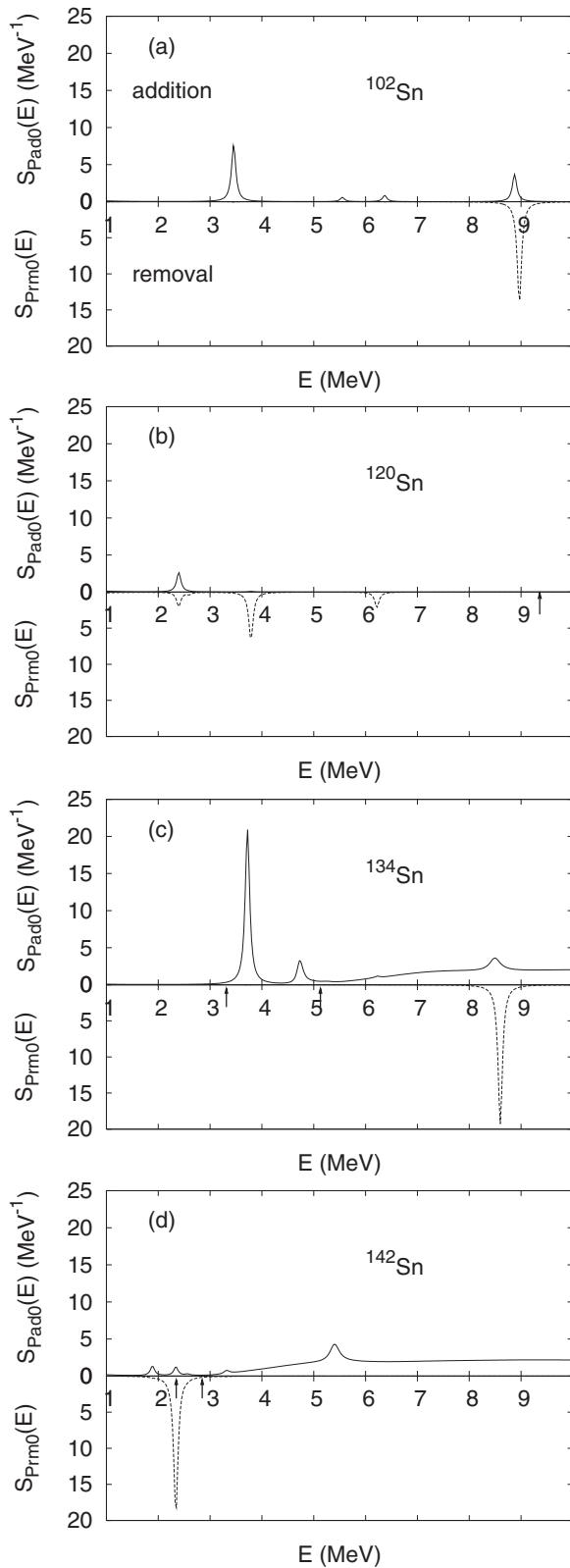


FIG. 3. The strength function  $S_{\text{Pad}0}(E)$  for the pair-addition mode (plotted in the upper panel with the solid curve) and the strength function  $S_{\text{Prm}0}(E)$  for the pair-removal mode (the dashed curve in the lower panel) in (a)  $^{102}\text{Sn}$ , (b)  $^{120}\text{Sn}$ , (c)  $^{134}\text{Sn}$ , and (d)  $^{142}\text{Sn}$ . The arrows indicate the calculated one- and two-neutron separation energies  $S_{1n}$  and  $S_{2n}$ .

process. Since it does not correspond to “transfer” reaction, we do not analyze below. Concerning the pair-removal strength function, sharp and large peaks located around  $E = 9.1$  and  $8.6$  MeV are observed in Figs. 3(a) and 3(c), respectively. This is the so called giant pairing vibration [11,43–45]: it is a collective mode of removing two neutrons which occupy the single-particle orbits in the next major shell below the valence shell, that is, the orbits in the  $N = 50$ – $82$  shell in the case of  $^{134}\text{Sn}$ . In the cases of  $^{120}\text{Sn}$  and  $^{142}\text{Sn}$ , similar peaks exist, but at slightly higher energy, and are not seen in Figs. 3(b) and 3(d).

### B. Transition density

We show in Fig. 4 the pair-addition and -removal transition densities  $P_{i0}^{(\text{ad})}(r)$  and  $P_{i0}^{(\text{rm})}(r)$ , and the particle-hole transition density  $\rho_{i0}^{\text{ph}}(r)$  for neutrons, associated with the low-lying pair vibrational modes in (a)  $^{102}\text{Sn}$ , (b)  $^{120}\text{Sn}$ , (c)  $^{134}\text{Sn}$ , and (d)  $^{142}\text{Sn}$ . The volume element  $r^2$  is multiplied to these quantities in the plots.

A peculiar feature of the low-lying pair vibrational mode in  $^{134}\text{Sn}$  is clearly visible in Fig. 4 when it is compared with the results for  $^{102}\text{Sn}$  and  $^{120}\text{Sn}$ . In the cases of  $^{102}\text{Sn}$  and  $^{120}\text{Sn}$ , all of the three kinds of transition density have increased amplitudes around the nuclear surface,  $r \gtrsim R_{\text{rms}} + 3$  fm ( $r \gtrsim 8$  fm). In  $^{134}\text{Sn}$ , however, the pair-addition transition density  $P_{i0}^{(\text{ad})}(r)$  has a significant amplitude even at  $r = R_{\text{rms}} + 3$  fm ( $r \approx 8$  fm) and a long tail extends up to  $r \approx 15$  fm. It is interesting to compare  $^{102}\text{Sn}$  and  $^{134}\text{Sn}$  [Fig. 4(a) vs 4(c)] since both cases commonly have the closed-shell plus two-neutron configuration. Although the maximum amplitudes in the two cases are about the same, the transition density in  $^{134}\text{Sn}$  significantly extends toward outside, resulting in the noticeable increase of the pair-addition transfer strength in  $^{134}\text{Sn}$ , that is,  $B(\text{Pad}0) = 3.16$ , which is larger by a factor of three than  $B(\text{Pad}0) = 1.18$  in  $^{102}\text{Sn}$ . We thus find that the spatial extension of the transition amplitude plays a central role to enhance the pair-addition transfer strength  $B(\text{Pad}0)$  in  $^{134}\text{Sn}$ .

The low-lying pair vibrational mode in  $^{142}\text{Sn}$  exhibits also an extended profile in the transition density, but in this case the dominant amplitude is the pair-removal transition density  $P_{i0}^{(\text{rm})}(r)$  and its spatial extension is smaller (observed up to  $r \sim 11$  fm) than that of  $P_{i0}^{(\text{ad})}(r)$  in  $^{134}\text{Sn}$ .

### C. Microscopic origin

In order to clarify the microscopic origin of the anomalous pair vibrational mode in  $^{134}\text{Sn}$ , we show in Fig. 5(a) effects of the residual pairing interaction on the pair-addition strength function  $S_{\text{Pad}0}(E)$ . Plotted here is the strength function associated with unperturbed neutron two-quasiparticle excitations, that is, the strength obtained by neglecting the residual interaction, and it is compared with the result of the full QRPA calculation. The first peak at  $E \approx 1.5$  MeV and the second one at  $E \approx 4.5$  MeV correspond to the two-quasineutron excitations  $[2f_{7/2}]^2$  and  $[3p_{3/2}]^2$ , respectively. The strengths

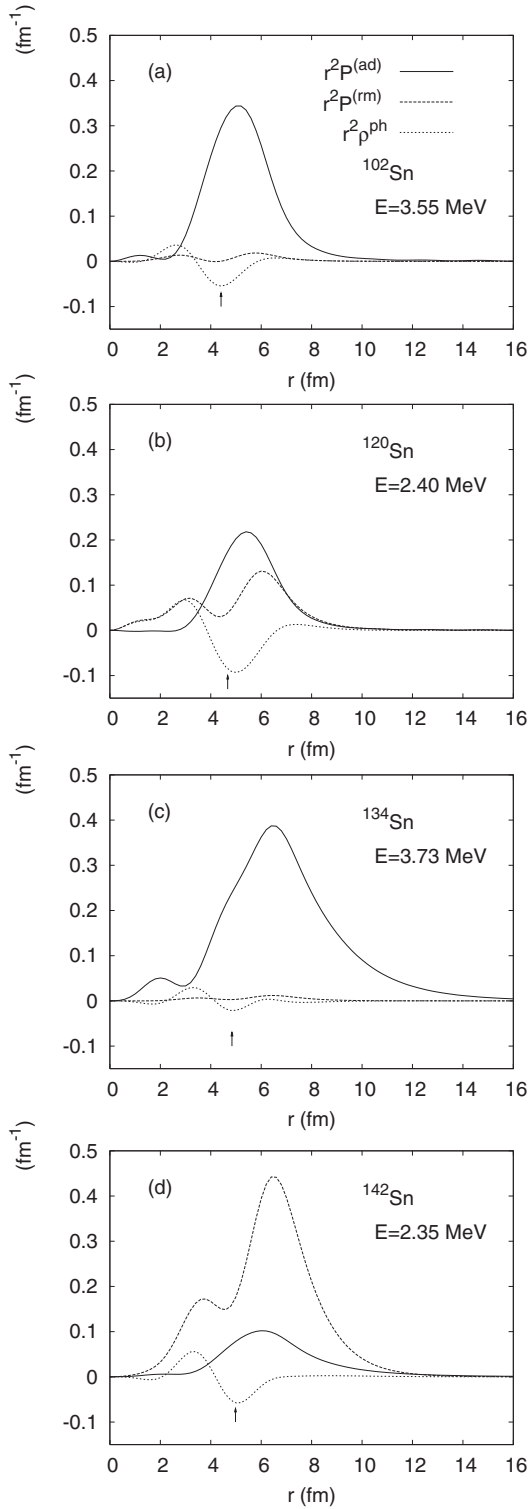


FIG. 4. (a) The neutron transition densities associated with the pair vibrational mode at  $E = 3.55$  MeV in  $^{102}\text{Sn}$ . The solid, the dashed, and the dotted curves represent the pair-addition transition density  $r^2 P_{i0}^{(\text{ad})}(r)$ , the pair-removal transition density  $r^2 P_{i0}^{(\text{rm})}(r)$ , and the particle-hole transition density  $r^2 \rho_{i0}^{\text{ph}}(r)$ , respectively. (b)–(d) The same as (a) but for  $^{120}\text{Sn}$ ,  $^{134}\text{Sn}$ , and  $^{142}\text{Sn}$ , respectively. The position of the arrow indicate the the root mean square radius  $R_{\text{rms}} = \sqrt{\langle r^2 \rangle}$  of the total nucleon density, which are 4.41, 4.67, 4.84, and 4.98 fm in  $^{102}\text{Sn}$ ,  $^{120}\text{Sn}$ ,  $^{134}\text{Sn}$ , and  $^{142}\text{Sn}$ , respectively.

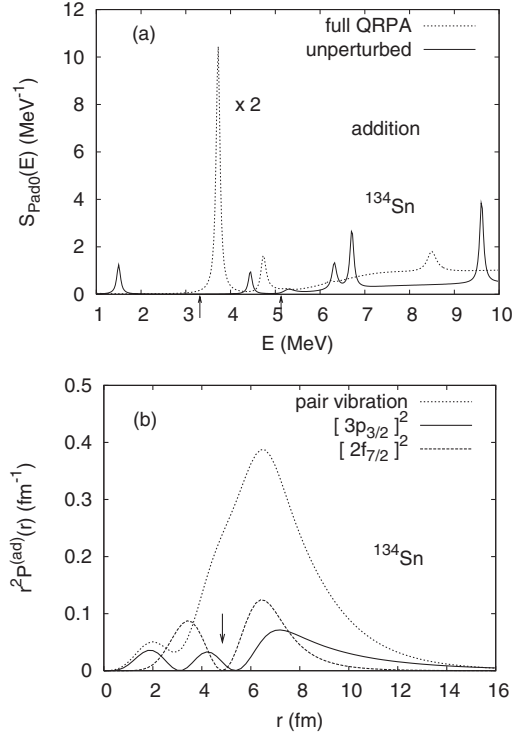


FIG. 5. (a) The pair-addition strength function  $S_{\text{Pad0}}(E)$  in  $^{134}\text{Sn}$ , calculated for the unperturbed neutron two-quasiparticle excitations (plotted with the solid curve) and in the full QRPA (dotted curve). (b) The transition density  $r^2 P_{i0}^{(\text{ad})}(r)$  of the unperturbed neutron two-quasiparticle excitations  $[2f_{7/2}]_2^2$  (solid curve) and  $[3p_{3/2}]_2^2$  (dashed curve) in  $^{134}\text{Sn}$ , compared with the transition density of the low-lying pair vibrational mode obtained in the full QRPA (dotted curve).

of these peaks are  $B(\text{Pad0}) = 0.18$  and  $0.15$  for  $[2f_{7/2}]_2^2$  and  $[3p_{3/2}]_2^2$ , respectively, and they are comparable to a single-particle estimate  $B_{\text{s.p.}}(\text{Pad0}) = (2j + 1)/8\pi$ . The large low-lying strength does not show up in the unperturbed strength, indicating that the collective configuration mixing caused by the residual interaction plays a crucial role to bring about the large strength of the pair vibrational mode in the full QRPA calculation. The collective enhancement is a factor of 20 as is estimated from the ratio of the strengths (3.16 vs 0.18, 0.15).

Figure 5(b) shows the pair-addition transition densities  $P_{i0}^{(\text{ad})}(r)$  associated with unperturbed neutron two-quasiparticle excitations  $[2f_{7/2}]_2^2$  and  $[3p_{3/2}]_2^2$ . It is seen that the transition density of the  $[3p_{3/2}]_2^2$  configuration has a long tail, extending up to  $r \sim 15$  fm. We here note that the quasiparticle energy of the neutron  $2f_{7/2}$  and  $3p_{3/2}$  states in  $^{134}\text{Sn}$  are 0.75 and 2.25 MeV, and the energies of the corresponding Hartree-Fock single-particle orbits are  $e_{\text{HF}} = -2.14$  and  $-0.36$  MeV, respectively. Here the binding energy of the  $3p_{3/2}$  orbit is only one fifth of that of  $2f_{7/2}$ , and is smaller than those of the single-particle orbits below the  $N = 82$  gap ( $e_{\text{HF}} < -7.77$  MeV) by a factor of 20. Clearly the long tail associated with the  $[3p_{3/2}]_2^2$  configuration is a consequence of the weak binding of the  $3p_{3/2}$  quasineutron state.

We speculate that many two-quasiparticle configurations including  $[3p_{3/2}]_2^2$  and  $[2f_{7/2}]_2^2$  contribute to produce the pair

vibrational mode in  $^{134}\text{Sn}$  as the transition density is larger by several times than those of the individual unperturbed two-quasiparticle excitations. Comparing the transition density of  $[3p_{3/2}]^2$  with that of the pair vibrational mode, we deduce that the long tail in the pair vibrational mode may be inherited from that of  $[3p_{3/2}]^2$ . Two-quasineutron configurations in the continuum, including the next lying  $3p_{1/2}$  unbound resonance state (located at positive energies around 0.2 MeV) may contribute also. Considering the orthogonality of the wave function of the pair vibrational mode to that of the pair rotational mode whose main component is  $[2f_{7/2}]^2$ , we deduce that the  $[3p_{3/2}]^2$  and  $[3p_{1/2}]^2$  configurations are the largest components in the pair vibrational mode. The mechanism of the long tail arising from the weak binding of the  $3p$  single-particle orbits may be analogous to the halo phenomena, where the weakly bound  $s$  and  $p$  orbits are known to play a central role, but it is interesting to note that the present case is not the ground state but the excited  $0^+$  state.

In Fig. 6(a) we plot the pair-removal strength function arising from unperturbed neutron two-quasiparticle excitations in  $^{142}\text{Sn}$ . The low-lying peak seen at  $E = 3.3$  MeV is the  $[2f_{7/2}]^2$  two-quasiparticle configurations, corresponding to creating two holes (i.e., removing two neutrons) in the  $2f_{7/2}$  orbit. There are also peaks associated with the unperturbed  $[3p_{3/2}]^2$  and  $[3p_{1/2}]^2$  configurations, which are however hardly visible in this scale. It is seen that the strength of the pair vibrational

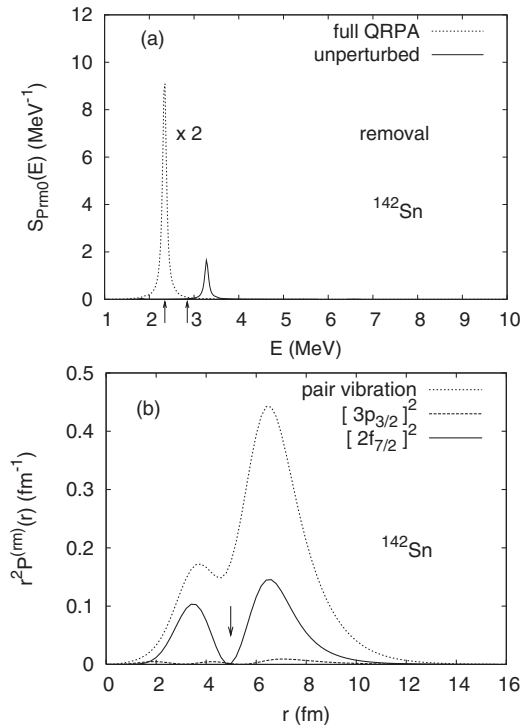


FIG. 6. (a) The pair-removal strength function  $S_{\text{Prm}0}(E)$  in  $^{142}\text{Sn}$ , calculated for the unperturbed neutron two-quasiparticle excitations (solid curve) and in the full QRPA (dotted curve). (b) The transition density  $r^2 P_{i0}^{(\text{rm})}(r)$  of the unperturbed neutron two-quasiparticle excitations  $[2f_{7/2}]^2$  (solid curve) and  $[3p_{3/2}]^2$  (dashed curve) in  $^{142}\text{Sn}$ , compared with the transition density of the low-lying pair vibrational mode obtained in the full QRPA (dotted curve).

mode in the full QRPA calculation is ten times larger than the unperturbed strength, indicating a collective effect. The transition densities of the two-quasiparticle configurations  $[2f_{7/2}]^2$  and  $[3p_{3/2}]^2$  are shown in Fig. 6(b). Comparison of the full and the unperturbed transition densities suggests that  $[2f_{7/2}]^2$  is one of the main configurations, but a significant mixing of configurations other than  $[2f_{7/2}]^2$  is also present. Since it is the pair-removal mode the configuration mixing involving those below the  $N = 82$  shell gap can contribute, but the weakly bound and continuum orbits such as  $3p_{3/2}$  and  $3p_{1/2}$  contribute very little to the pair removal mode as their occupation are small. Consequently the spatial extension of the transition density of the pair-removal vibrational mode in  $^{142}\text{Sn}$  is smaller than that of the pair-addition vibrational mode in  $^{134}\text{Sn}$ .

#### D. Systematics

It is interesting to see systematical behavior of the low-lying pair vibrational modes along the isotopic chain of Sn. Here we treat separately the pair-addition and the pair-removal modes of the pairing vibration. They are identified as the QRPA eigenmode having the largest pair-addition (pair-removal) strength among the peaks below  $E = 5$  MeV.

In Fig. 7 and Table I are shown the excitation energy and the pair-addition strength  $B(\text{Pad}0)$  of the low-lying pair-addition vibrational modes. (We plot here the results obtained with the DDDI-bare', the mix and the volume pairing interactions, but we shall discuss dependence on the pair interaction later.) We also plot in Fig. 7(a) the calculated threshold energies  $S_{1n}$  and  $S_{2n}$  of one- and two-neutron separations. A noticeable feature is that in the isotopes with  $A > 132$  the low-lying pair vibrational modes are located near the neutron separation energies. This is due to the sudden decrease of the separation energies in isotopes beyond the magic number  $N = 82$ . The minimum at  $A = 140$  ( $N = 90$ ) reflects the subshell closure of the  $2f_{7/2}$  orbit. In Fig. 7(b), large pair-addition strength  $B(\text{Pad}0)$  is seen in five isotopes with  $A = 132$ – $140$  ( $N = 82$ – $90$ ).

Figure 8 shows the pair-addition transition density  $P_{i0}^{(\text{ad})}(r)$  of the low-lying pair-addition vibrational modes in the isotopes from  $A = 120$  (a stable isotope) to  $A = 150$ . We find that the pair vibrational modes in the  $A = 132$ – $140$  isotopes have quite similar radial profiles of the transition density  $P_{i0}^{(\text{ad})}(r)$ , and they all share the common character concerning the spatial extension reaching  $r \sim 15$  fm. These features all indicate that the anomalous pair vibrational mode appears systematically in the region beyond the  $N = 82$  magic number and up to  $N = 90$ . It is also evident that the anomalous pair vibrational modes in  $A = 132$ – $140$  are distinct from those in the  $A = 120$ – $130$  isotopes closer to the stability line.

Systematics of the pair-removal vibrational mode is shown in Fig. 9 and also in Table I. The excitation energy and the pair-removal strength  $B(\text{Prm}0)$  are plotted in Figs. 9(a) and 9(b), respectively. In the isotopes with  $A = 134$ – $140$ , the low-lying pair-removal strength is negligible. However, the pair-removal vibrational mode having large strength emerges in the isotopes beyond  $A = 140$  ( $N = 90$ ). It is found that the pair

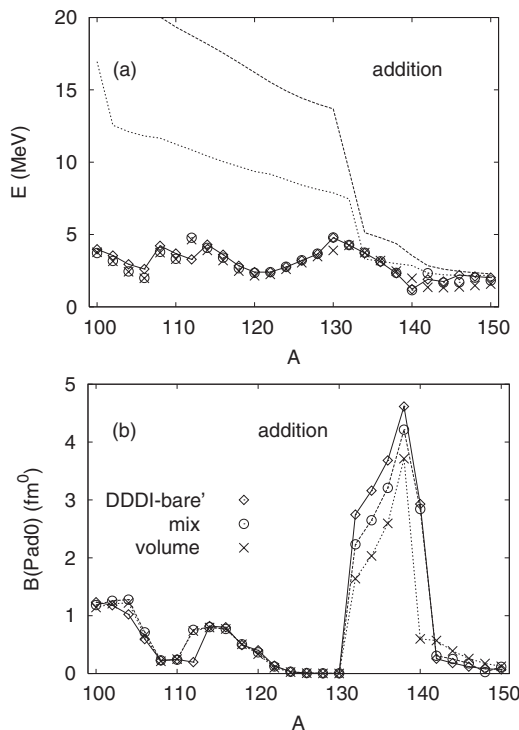


FIG. 7. (a) The excitation energy of the pair-addition vibrational mode. The one- and two-neutron separation energies are plotted with the dotted and the dashed lines, respectively. (b) The pair-addition strength  $B(\text{Pad}0)$  of the pair-addition vibrational mode. The diamonds connected with the solid line are the results obtained with the pairing interaction DDDl-bare' while the circles and the crosses are those with the mix and the volume pairing interactions, respectively.

vibrational mode in these isotopes have the same character which we discussed in connection with the results for  $^{142}\text{Sn}$  [cf. Fig. 4(d)].

### E. Comparison with pair rotational ground-state transition

The anomalous feature of the pair vibrational modes in  $A = 132$ – $140$  is clarified further by comparing the pair vibration with the pair transfer populating the ground state, that is, the pairing rotation discussed in Sec. III.

Figure 10(a) show the ratio  $r = B(\text{Pad}0; \text{gs} \rightarrow \text{pv}) / B(\text{Pad}0; \text{gs} \rightarrow \text{gs})$  of the pair-addition strength associated with the low-lying pair vibrational mode and that with the pair rotational ground-state transfer. The strength ratio amounts to 60%–90% in the  $A = 132$ – $140$  isotopes. It is compared with isotopes in the middle of the  $N = 50$ – $82$  shell, where the ratio is far below 10% (except in a few isotopes at the beginning of the shell). The small ratio in the isotopes  $A \sim 110$ – $130$  is in qualitative agreement with the well established observation that two-neutron transfer cross sections populating low-lying  $0^+$  states is generally weak, for instance, less than 10% in stable Sn isotopes [8,12]. A known exception is the case where an excited  $0^+$  state having the character of the shape coexistence emerges as a consequence of sudden shape changes with the neutron number [8,46]. The large strength

TABLE I. The pair-addition and pair-removal strengths  $B(\text{Pad}/\text{rm}0)$  of the ground-state transition, the excitation energy  $E$  and the pair-addition strength  $B(\text{Pad}0)$  of the pair-addition vibrational mode, and the excitation energy  $E$  and the pair-removal strength  $B(\text{Prm}0)$  of the pair-removal vibrational mode in Sn isotopes. The unit of the excitation energy is MeV. The ground-state transitions in the closed shell nuclei  $^{100}\text{Sn}$  and  $^{132}\text{Sn}$  are evaluated in the QRPA, separately for the pair-addition and pair-removal transitions.

A	Ground state $B(\text{Pad}/\text{rm}0)$	p.v. addition		p.v. removal	
		$E$	$B(\text{Pad}0)$	$E$	$B(\text{Prm}0)$
100	3.096(a)	3.99	1.233		
102	3.138	3.55	1.180	3.55	0.003
104	5.101	2.95	1.023	2.95	0.037
106	6.498	2.62	0.595	2.62	0.183
108	7.857	4.22	0.225	2.82	0.370
110	8.932	3.69	0.245	3.28	0.405
112	9.872	3.28	0.198	3.81	0.435
114	9.798	4.30	0.820	4.30	0.448
116	9.333	3.61	0.800	2.78	0.488
118	8.855	2.84	0.493	3.25	0.888
120	8.274	2.40	0.402	3.80	0.984
122	7.851	2.40	0.136	4.63	0.920
124	7.374	2.75	0.031	2.75	0.699
126	6.462	3.20	0.010	3.20	0.625
128	4.991	3.65	0.004	3.65	0.557
130	2.851	4.78	0.005	4.78	0.498
132	3.202(r) 3.973(a)	4.28	2.747	4.43	0.458
134	3.607	3.73	3.160	3.73	0.000
136	5.662	3.10	3.683	3.10	0.007
138	6.048	2.33	4.615	2.33	0.058
140	5.157	1.23	2.929	1.23	2.376
142	11.079	1.90	0.256	2.35	2.800
144	16.088	1.75	0.182	3.10	1.983
146	19.869	2.20	0.119	3.65	1.563
148	22.639	2.10	0.082	4.08	1.338
150	24.481	2.03	0.071	4.45	1.077

ratio of 60%–90% in the  $A = 132$ – $140$  isotopes is comparable with the cases of the shape transition and shape coexistence.

In Fig. 10(b) we compare the pair-addition transition densities  $P_{i0}^{(\text{ad})}(r)$  for the ground-state transitions and for the pair vibrational transitions populating excited  $0^+$  states, calculated for  $^{134}\text{Sn}$ . The maximal values of the amplitudes are comparable, but the transition density of the anomalous pair vibration mode extends more than that associated with the pair rotational ground-state transition. It reflects different microscopic structures of the pairing rotation and of the anomalous pairing vibration. As we discussed in connection with Fig. 2, the largest component of the pairing rotation may be  $[2f_{7/2}]^2$ , while the counterpart of the anomalous pairing vibration may be  $[3p_{3/2}]^2$  and  $[3p_{2/1}]^2$ . The  $3p$  orbits have much smaller binding energy and thus longer tail in the wave functions than those of  $2f_{7/2}$ . The difference in the spatial extension of the transition densities may be explained in this context. Here we remind the reader again that the excited  $0^+$  state associated with the anomalous pair vibrational mode is located very close to the neutron separation energy (the energy

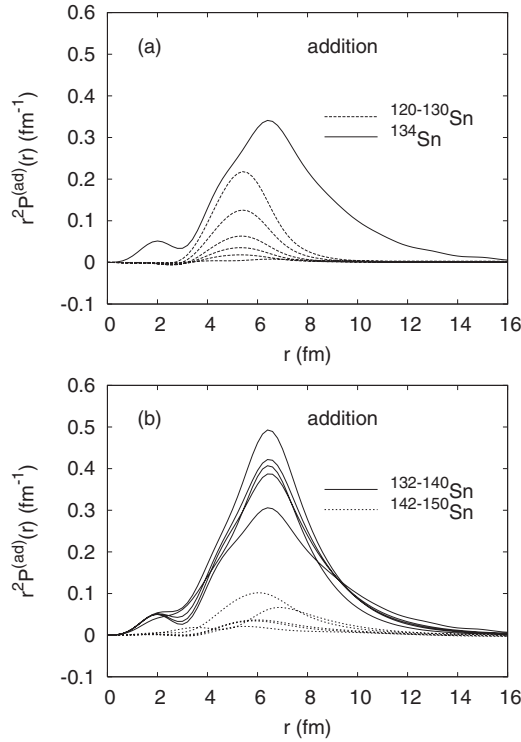


FIG. 8. The pair-addition transition density  $r^2 P_{i0}^{(ad)}(r)$  associated with the pair-addition vibrational mode (a) in  $^{120-130}\text{Sn}$  and  $^{134}\text{Sn}$  and (b) in  $^{132-140}\text{Sn}$  and  $^{142-150}\text{Sn}$ . The effective pairing interaction is the DDDI-bare’.

difference is less than  $\sim 1$  MeV in  $^{134-140}\text{Sn}$ ). It implies that the binding energy of neutrons forming the excited  $0^+$  state is significantly smaller than neutrons forming the ground state. Therefore, the longer tail of the anomalous pair vibrational mode than that of the ground-state transfer can be ascribed to the weaker binding of the excited  $0^+$  states. The microscopic key is of course the presence of the weakly bound  $3p$  orbits in which the transferred two neutrons are accommodated.

The ratio  $r' = B(\text{Prm}0; \text{gs} \rightarrow \text{pv})/B(\text{Prm}0; \text{gs} \rightarrow \text{gs})$  of the strengths of the pair-removal vibrational mode and of the pairing rotation is shown in Fig. 10(c). The ratio in  $^{140-142}\text{Sn}$  is 30%–40%, but it is relatively small if compared to the ratio 60%–90% of the pair addition strengths in  $^{132-140}\text{Sn}$ , and it decreases to small values in  $A > 144$ . Note that in the isotopes beyond  $A = 140$  the strengths of the pair rotational ground-state transfer is more drastically increased than the strengths of the pair-removal vibrational mode.

## V. SENSITIVITY TO DENSITY-DEPENDENT PAIRING

It is interesting to examine the sensitivity of the pair transfers to different effective pairing interactions [21,23]. For this purpose we have performed the HFB + QRPA calculations with the three different versions of the DDDI described in Sec. II A. Note that the three interactions are designed to give approximately the same values of the average neutron pair gap  $\Delta_{uv}$  [cf. Fig. 1(b)]. Comparing the three interactions, we can

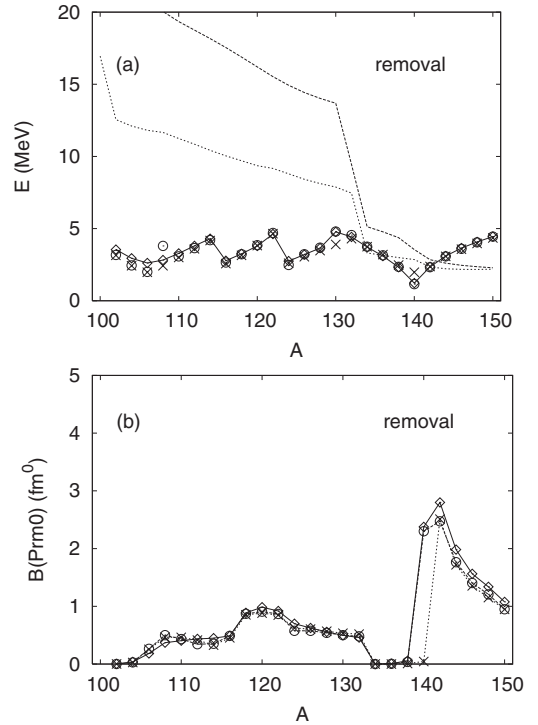


FIG. 9. (a) The excitation energy and (b) the pair-removal strength  $B(\text{Prm}0)$  of the pair-removal vibrational mode. See also the caption of Fig. 7.

examine effects of different density dependences of the DDDI while keeping approximately the same average pair gap.

The influence of the density dependence on the pair-addition and pair-removal strengths  $B(\text{Pad}/\text{rm}0)$  of the ground-state transition is shown in Fig. 1(a). Although the influence is not significant for  $A = 100-132$ , we see some sensitivity to the density dependence for neutron-rich isotopes with  $A > 132$ .

Concerning the pair vibrational modes, in contrast, the anomalous pairing vibration in  $A = 132-140$  has significant sensitivity to the density dependence of the effective pairing interactions. As an example, we show in Fig. 11(a) the pair-addition strength function  $S_{\text{Pad}0}(E)$  in  $^{134}\text{Sn}$  calculated with the three different DDDIs. It is noticed that the basic structure of the strength function is the same, and the anomalous pair vibrational mode commonly exists at  $E = 3.73-3.75$  MeV. More importantly it is seen that the height of the pair vibrational peak depends strongly on the different pairing interaction by about a factor of 1.5; the pair-addition strength is  $B(\text{Pad}/\text{rm}0) = 3.16, 2.65,$  and  $2.03$  for the DDDI-bare’, mix, and volume pairing interactions, respectively. The difference is larger than that found in the ground-state transition. The same effect is seen commonly at  $A = 132-138$  as shown in Fig. 7(b). On the other hand, the influence of the density dependence on the pair-addition vibrational in the isotopes  $A < 132$  mode is small.

We can understand the influence of the density dependence on the anomalous pair vibrational mode in terms of the transition density  $P_{i0}^{(ad)}(r)$ , whose dependence on the pair interactions is shown in Fig. 11(b). It is seen in this figure

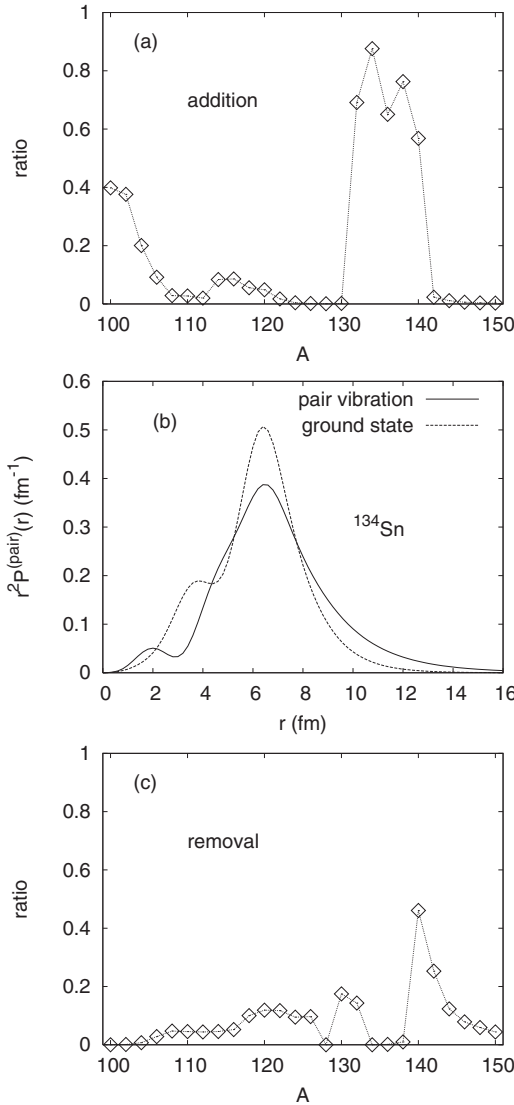


FIG. 10. (a) The ratio of the pair-addition strength  $B(\text{Pad}0; \text{gs} \rightarrow \text{pv})$  of the low-lying pair-addition vibrational mode and the strength  $B(\text{Pad}0; \text{gs} \rightarrow \text{gs})$  of the ground-state transfer. (b) The pair-addition transition density  $r^2 P_{i0}^{(\text{ad})}(r)$  associated with the anomalous pair vibrational mode (solid curve) and that for the ground-state transfer (dashed curve) in  $^{134}\text{Sn}$ . (c) The ratio of the pair-removal strength  $B(\text{Prm}0; \text{gs} \rightarrow \text{pv})$  of the low-lying pair-removal mode and the ground-state transfer strength  $B(\text{Pad}0; \text{gs} \rightarrow \text{gs})$ .

that the amplitude  $P_{i0}^{(\text{ad})}(r)$  in the external region  $r \gtrsim R_{\text{rms}}$  outside the surface shows the same trend as in the pair-addition strength  $B(\text{Pad}0)$ ; the DDDI-bare' > mix > volume pairing interactions. We can then relate this trend to the features of the interaction strength  $V_n(r)$ , which is, in the external region, the largest for the DDDI-bare' and the smallest for the volume pairing, reflecting the interaction strength at low densities. ( $v_0 = -458, -292, -195$  MeV fm $^3$  and see also Fig. 1 of Ref. [23]). Since the anomalous pair vibrational mode at  $A = 132-140$  has the transition density extending far outside the surface, the large difference in the interaction strength  $V_n(r)$  in the exterior is effective to this mode. However, for the

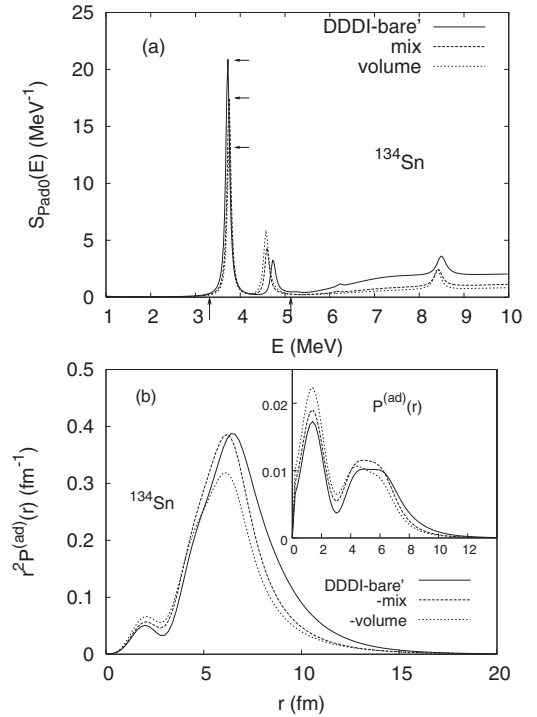


FIG. 11. (a) The pair-addition strength function  $S_{\text{Pad}0}(E)$  for neutrons in  $^{134}\text{Sn}$ , calculated with the three effective pairing interactions; the DDDI-bare', the mix, and the volume types. The arrows indicate the peak heights. (b) The transition density  $r^2 P_{i0}^{(\text{ad})}(r)$  of the low-lying pair-addition vibrational mode in  $^{134}\text{Sn}$ , calculated with the three effective pairing interactions; the DDDI-bare', mix, and volume types. In the inset we show the transition density  $P_{i0}^{(\text{ad})}(r)$  without the volume element.

usual pair vibrational modes whose transition density does not reach very far, the sensitivity becomes small.

Finally we remark on related works [21,23] discussing the sensitivity to the density dependence of the effective pairing interaction. In Ref. [21], the pair-transfer strengths and the transition density of the pair vibrational modes are analyzed for  $^{124}\text{Sn}$  and  $^{136}\text{Sn}$  by using the Skyrme-HFB + QRPA model, which is similar to the model adopted here. In the case of  $^{136}\text{Sn}$ , the low-lying pair vibrational mode around  $E \sim 3$  MeV emerges in two of their calculations (the  $\eta = 0.65$  and  $0.35$  cases of Ref. [21]), in qualitative agreement with our results. The shape of the pair-addition transition density  $P_{i0}^{(\text{ad})}(r)$  is also similar as seen from the comparison of the inset of Fig. 11(b) of the present paper and Fig. 8 of Ref. [21]. On the other hand, in another calculation adopting the DDDI with the strongest density dependence (the  $\eta = 1$  case in Ref. [21]), the low-lying pair vibrational mode is fragmented into three peaks (cf. Fig. 7 of Ref. [21]), suggesting a complex sensitivity to the pairing interactions. We note that the interaction strength  $v_0 = -670$  MeV fm $^3$  chosen in the  $\eta = 1$  case is too large since it leads to the positive scattering length, implying unphysical existence of a bound state for the  $S = 0$  neutron pair. For comparison, we have performed a calculation using the surface interaction, which is defined by Eq. (2) where  $\eta = 1$ ,  $\rho_c = 0.16$ , and the neutron density is replaced with

the total density, as is adopted in Ref. [21]. Choosing the interaction strength  $v_0$  in our way, that is, to reproduce the neutron pairing gap in  $^{120}\text{Sn}$ , we have  $v_0 = -478.5 \text{ MeV fm}^3$ . The QRPA response with this pairing interaction produces a single-peak pair vibrational mode with  $E = 3.90 \text{ MeV}$  and  $B(\text{Pad}/\text{rm}0) = 3.02$ , which are very close to the DDDI-bare' result in Table I. This close similarity can be understood as the interaction strength  $v_0$  in our surface interaction is almost identical to that of the DDDI-bare', indicating similar density dependence of the pairing interaction.

It is discussed in Ref. [23] that the quadrupole pair-addition transfer populating the first  $2^+$  states in  $^{134}\text{Sn}$  and heavier isotopes is sensitive to the density dependence of the pairing interaction. In that case the ratio of the pair-addition strengths between the volume pairing and the DDDI-bare' amounts to approximately a factor of 2, which is slightly larger than the sensitivity (a factor of  $\sim 1.5$ ) of the pair vibrational mode in  $^{132-140}\text{Sn}$ . The origin of the different sensitivity is not clear at present, but it may be related to the fact that the monopole pair transition density also has larger amplitude in the internal region of the nucleus than that of the quadrupole mode.

## VI. CONCLUSIONS

We have investigated microscopically monopole two-neutron transfer modes in heavy-mass superfluid nuclei using the Skyrme-Hartree-Fock-Bogoliubov mean-field model and the continuum quasiparticle random phase approximation. Emphases have been put on the pair vibrational modes populating low-lying collective  $0^+$  states and on the pair rotational transitions connecting the ground states of the neighboring  $\Delta N = \pm 2$  isotopes. We have performed systematic numerical analysis for the even-even Sn isotopes ranging from  $A = 100$  to  $A = 150$ , and found the following new features of the two-neutron transfer modes emerging in neutron-rich Sn isotopes beyond the  $N = 82$  shell closure ( $A > 132$ ).

The calculation predicts an anomalous pair vibrational mode in the isotopes  $^{132-140}\text{Sn}$ . It is a monopole vibrational mode characterized by intense transition from the ground state to a low-lying  $0^+$  state in the neighboring  $N + 2$  isotope via the two-neutron addition transfer. The corresponding  $0^+$

states are predicted to emerge near the threshold energy of the one-neutron separation, and to form a narrow resonance if it is located above the separation energy. An anomalous feature of this pair vibrational mode and a marked difference from the pairing vibration in nuclei near the stability line is that the pair transition density exhibits a large amplitude in the region outer than the surface, and also a long tail extending up to  $r \sim 15 \text{ fm}$ . We expect that the difference may manifest itself in reaction observables such as the cross section of the  $(t, p)$  reaction although quantitative analysis remains for future investigations. As a microscopic origin of the anomalous pair vibrational mode, the weakly bound or resonant  $3p_{3/2}$  and  $3p_{1/2}$  orbits are suggested to play key roles.

We have also studied how the predicted anomalous pair vibration depends on the effective pairing interaction. It is found that the anomalous features are significant if we adopt the density-dependent  $\delta$  interaction which exhibits increased interaction strength in the external low density region (so that it reproduces the large scattering length of the  $^1S$  bare nuclear force). The increased interaction strength at outside is one of the key factors that causes the anomalous pair vibration.

In very neutron-rich isotopes with  $A > 140$  ( $N > 90$ ), enhancement of the two-neutron transfer strength is predicted for the transitions between the ground states. This is a natural consequence of the spatially extended pair field originating from the weak binding of neutrons. Particularly, occupation of the weakly bound  $3p_{3/2}$  and  $3p_{1/2}$  orbits gives the sudden increase in the strength for  $A > 140$ . In this perspective, the anomalous pair vibrational mode in  $^{132-140}\text{Sn}$  can be linked to the strong ground-state transfer in  $A > 140$ , and it can be regarded as a precursor of the enhanced pair transfer which emerges in weakly bound neutron-rich nuclei close to the drip line.

## ACKNOWLEDGMENTS

This work was supported by the Grant-in-Aid for Scientific Research (Nos. 20540259, 21105507, 21340073, and 23540294) from the Japan Society for the Promotion of Science, and also by the JSPS Core-to-Core Program, International Research Network for Exotic Femto Systems (EFES).

- 
- [1] N. Keeley *et al.*, *Phys. Lett. B* **646**, 222 (2007).
  - [2] I. Tanihata *et al.*, *Phys. Rev. Lett.* **100**, 192502 (2008).
  - [3] A. Chatterjee *et al.*, *Phys. Rev. Lett.* **101**, 032701 (2008).
  - [4] M. S. Golovkov *et al.*, *Phys. Lett. B* **672**, 22 (2009).
  - [5] A. Lemasson *et al.*, *Phys. Lett. B* **697**, 454 (2011).
  - [6] S. Yoshida, *Nucl. Phys.* **33**, 685 (1962).
  - [7] D. R. Bes and R. A. Broglia, *Nucl. Phys.* **80**, 289 (1966).
  - [8] R. A. Broglia, O. Hansen, and C. Riedel, in *Advances in Nuclear Physics*, edited by M. Baranger and E. Vogt (Plenum, New York, 1973), Vol. 6, pp. 287–457.
  - [9] A. Bohr and B. R. Mottelson, *Nuclear Structure* (Benjamin, New York, 1975), Vol. II.
  - [10] M. Igarashi, K.-I. Kubo, and K. Yagi, *Phys. Rep.* **199**, 1 (1991).
  - [11] W. von Oertzen and A. Vitturi, *Rep. Prog. Phys.* **64**, 1247 (2001).
  - [12] D. M. Brink and R. A. Broglia, *Nuclear Superfluidity: Pairing in Finite Systems* (Cambridge University Press, Cambridge, 2005).
  - [13] G. F. Bertsch and H. Esbensen, *Ann. Phys.* **209**, 327 (1991); H. Esbensen and G. F. Bertsch, *Nucl. Phys. A* **542**, 310 (1992).
  - [14] U. Lombardo and H.-J. Schulze, *Lecture Notes in Physics* (Springer, Berlin, 2001), Vol. 578, p. 30.
  - [15] D. J. Dean and M. Hjorth-Jensen, *Rev. Mod. Phys.* **75**, 607 (2003).
  - [16] M. Matsuo, *Phys. Rev. C* **73**, 044309 (2006).
  - [17] J. Margueron, H. Sagawa, and K. Hagino, *Phys. Rev. C* **77**, 054309 (2008).
  - [18] T. Abe and R. Seki, *Phys. Rev. C* **79**, 054002 (2009).
  - [19] A. Gezerlis and J. Carlson, *Phys. Rev. C* **81**, 025803 (2010).

- [20] J. Dobaczewski, W. Nazarewicz, T. R. Werner, J. F. Berger, C. R. Chinn, and J. Dechargé, *Phys. Rev. C* **53**, 2809 (1996).
- [21] E. Khan, M. Grasso, and J. Margueron, *Phys. Rev. C* **80**, 044328 (2009).
- [22] E. Pllumbi, M. Grasso, D. Beaumel, E. Khan, J. Margueron, and J. van de Wiele, *Phys. Rev. C* **83**, 034613 (2011).
- [23] M. Matsuo and Y. Serizawa, *Phys. Rev. C* **82**, 024318 (2010).
- [24] G. Potel, B. F. Bayman, F. Bracco, E. Vigezzi, and R. A. Broglia, [arXiv:0906.4298](https://arxiv.org/abs/0906.4298).
- [25] G. Potel, F. Barranco, E. Vigezzi, and R. A. Broglia, *Phys. Rev. Lett.* **105**, 172502 (2010).
- [26] E. Khan, N. Sandulescu, N. V. Giai, and M. Grasso, *Phys. Rev. C* **69**, 014314 (2004).
- [27] B. Avez, C. Simenel, and Ph. Chomaz, *Phys. Rev. C* **78**, 044318 (2008).
- [28] M. Bender, P.-H. Heenen, and P.-G. Reinhard, *Rev. Mod. Phys.* **75**, 121 (2003).
- [29] M. Matsuo, *Nucl. Phys. A* **696**, 371 (2001); *Prog. Theor. Phys. Suppl.* **146**, 110 (2002).
- [30] Y. Serizawa and M. Matsuo, *Prog. Theor. Phys.* **121**, 97 (2009).
- [31] E. Chabanat, P. Bonche, P. Haensel, J. Meyer, and R. Schaeffer, *Nucl. Phys. A* **635**, 231 (1998); **643**, 441 (1998).
- [32] R. R. Chasman, *Phys. Rev. C* **14**, 1935 (1976).
- [33] E. Garrido, P. Sarriguren, E. Moya de Guerra, and P. Schuck, *Phys. Rev. C* **60**, 064312 (1999).
- [34] E. Garrido, P. Sarriguren, E. Moya de Guerra, U. Lombardo, P. Schuck, and H. J. Schulze, *Phys. Rev. C* **63**, 037304 (2001).
- [35] J. Dobaczewski, W. Nazarewicz, and P.-G. Reinhard, *Nucl. Phys. A* **693**, 361 (2001).
- [36] J. Dobaczewski and W. Nazarewicz, *Prog. Theor. Phys. Suppl.* **146**, 70 (2002).
- [37] J. Dobaczewski, W. Nazarewicz, and M. V. Stoitsov, *Euro. Phys. J. A* **15**, 21 (2002).
- [38] K. Hagino and H. Sagawa, *Phys. Rev. C* **72**, 044321 (2005).
- [39] M. Matsuo, Y. Serizawa, and K. Mizuyama, *Nucl. Phys. A* **788**, 307c (2007).
- [40] M. Yamagami, *Phys. Rev. C* **72**, 064308 (2005).
- [41] M. Yamagami, Y. R. Shimizu, and T. Nakatsukasa, *Phys. Rev. C* **80**, 064301 (2009).
- [42] W. Satula, J. Dobaczewski, and W. Nazarewicz, *Phys. Rev. Lett.* **81**, 3599 (1998).
- [43] R. A. Broglia and D. R. Bes, *Phys. Lett. B* **69**, 129 (1977).
- [44] M. W. Herzog, R. J. Liotta, and T. Vertse, *Phys. Lett. B* **165**, 35 (1985); M. W. Herzog, R. J. Liotta, and L. J. Sibanda, *Phys. Rev. C* **31**, 259 (1985).
- [45] P. Lotti, F. Cazzola, P. F. Bortignon, R. A. Broglia, and A. Vitturi, *Phys. Rev. C* **40**, 1791 (1989).
- [46] J. L. Wood, K. Heyde, W. Nazarewicz, M. Huyse, and P. van Duppen, *Phys. Rep.* **215**, 101 (1992).